

clamp and voltage-clamp recordings were made using a Multiclamp 700A amplifier (Axon Instruments). Patch pipettes (4–8 MΩ) were filled with a K-methanesulphonate-based internal solution (7 mM Cl<sup>-</sup>). Sensory responses were evoked by an air puff (30–300 ms, 60 p.s.i.) timed by a Picospritzer (General Valve) and delivered to the ipsilateral perioral surface. Data are represented as mean ± s.e.m. See Supplementary Methods for further details.

Received 12 January; accepted 26 February 2004; doi:10.1038/nature02442.

1. Eccles, J. C., Ito, M. & Szentagotai, J. *The Cerebellum as a Neuronal Machine* (Springer, Berlin, 1967).
2. Jakob, R. L. & Hamori, J. Quantitative morphology and synaptology of cerebellar glomeruli in the rat. *Anat. Embryol. (Berl.)* **179**, 81–88 (1988).
3. Konnerth, A., Llano, I. & Armstrong, C. M. Synaptic currents in cerebellar Purkinje cells. *Proc. Natl Acad. Sci. USA* **87**, 2662–2665 (1990).
4. Takechi, H., Eilers, J. & Konnerth, A. A new class of synaptic response involving calcium release in dendritic spines. *Nature* **396**, 757–760 (1998).
5. Perkel, D. J., Hestrin, S., Sah, P. & Nicoll, R. A. Excitatory synaptic currents in Purkinje cells. *Proc. R. Soc. Lond. B* **241**, 116–121 (1990).
6. Casado, M., Isope, P. & Ascher, P. Involvement of presynaptic N-methyl-D-aspartate receptors in cerebellar long-term depression. *Neuron* **33**, 123–130 (2002).
7. Wang, S. S.-H., Denk, W. & Häusser, M. Coincidence detection in single dendritic spines mediated by calcium release. *Nature Neurosci.* **3**, 1266–1273 (2000).
8. Brown, S. P., Brenowitz, S. D. & Regehr, W. G. Brief presynaptic bursts evoke synapse-specific retrograde inhibition mediated by endogenous cannabinoids. *Nature Neurosci.* **6**, 1048–1057 (2003).
9. Silver, R. A., Traynelis, S. F. & Cull-Candy, S. G. Rapid-time-course miniature and evoked excitatory currents at cerebellar synapses *in situ*. *Nature* **355**, 163–166 (1992).
10. Gabbiani, F., Midtgard, J. & Knöpfel, T. Synaptic integration in a model of cerebellar granule cells. *J. Neurophysiol.* **72**, 999–1009 (1994).
11. Shambes, G. M., Gibson, J. M. & Welker, W. Fractured somatotopy in granule cell tactile areas of rat cerebellar hemispheres revealed by micromapping. *Brain Behav. Evol.* **15**, 94–140 (1978).
12. Bower, J. M. & Woolston, D. C. Congruence of spatial organization of tactile projections to granule cell and Purkinje cell layers of cerebellar hemispheres of the albino rat: vertical organization of cerebellar cortex. *J. Neurophysiol.* **49**, 745–766 (1983).
13. Morissette, J. & Bower, J. M. Contribution of somatosensory cortex to responses in the rat cerebellar granule cell layer following peripheral tactile stimulation. *Exp. Brain Res.* **109**, 240–250 (1996).
14. D'Angelo, E., De Filippi, G., Rossi, P. & Taglietti, V. Synaptic excitation of individual rat cerebellar granule cells *in situ*: evidence for the role of NMDA receptors. *J. Physiol. (Lond.)* **484**, 397–413 (1995).
15. Brickley, S. G., Revilla, V., Cull-Candy, S. G., Wisden, W. & Farrant, M. Adaptive regulation of neuronal excitability by a voltage-independent potassium conductance. *Nature* **409**, 88–92 (2001).
16. Brickley, S. G., Cull-Candy, S. G. & Farrant, M. Development of a tonic form of synaptic inhibition in rat cerebellar granule cells resulting from persistent activation of GABA<sub>A</sub> receptors. *J. Physiol. (Lond.)* **497**, 753–759 (1996).
17. D'Angelo, E., De Filippi, G., Rossi, P. & Taglietti, V. Ionic mechanism of electroresponsiveness in cerebellar granule cells implicates the action of a persistent sodium current. *J. Neurophysiol.* **80**, 493–503 (1998).
18. Wall, M. J. & Usowicz, M. M. Development of action potential-dependent and independent spontaneous GABA<sub>A</sub> receptor-mediated currents in granule cells of postnatal rat cerebellum. *Eur. J. Neurosci.* **9**, 533–548 (1997).
19. Hamann, M., Rossi, D. J. & Attwell, D. Tonic and spillover inhibition of granule cells control information flow through cerebellar cortex. *Neuron* **33**, 625–633 (2002).
20. Stell, B. M., Brickley, S. G., Tang, C. Y., Farrant, M. & Mody, I. Neuroactive steroids reduce neuronal excitability by selectively enhancing tonic inhibition mediated by δ subunit-containing GABA<sub>A</sub> receptors. *Proc. Natl Acad. Sci. USA* **100**, 14439–14444 (2003).
21. Eccles, J. C., Faber, D. S., Murphy, J. T., Sabah, N. H. & Taborikova, H. Afferent volleys in limb nerves influencing impulse discharges in cerebellar cortex. I. In mossy fibers and granule cells. *Exp. Brain Res.* **13**, 15–35 (1971).
22. Garwicz, M., Jörntell, H. & Ekerot, C. F. Cutaneous receptive fields and topography of mossy fibres and climbing fibres projecting to cat cerebellar C3 zone. *J. Physiol. (Lond.)* **512**, 277–293 (1998).
23. Marr, D. A theory of cerebellar cortex. *J. Physiol. (Lond.)* **202**, 437–470 (1969).
24. Albus, J. S. A theory of cerebellar function. *Math. Biosci.* **10**, 25–61 (1971).
25. Wall, M. J. Endogenous nitric oxide modulates GABAergic transmission to granule cells in adult rat cerebellum. *Eur. J. Neurosci.* **18**, 869–878 (2003).
26. Krahe, R. & Gabbiani, F. Burst firing in sensory systems. *Nature Rev. Neurosci.* **5**, 13–23 (2004).
27. Lisman, J. E. Bursts as a unit of neural information: making unreliable synapses reliable. *Trends Neurosci.* **20**, 38–43 (1997).
28. Hahnloser, R. H., Kozhevnikov, A. A. & Fee, M. S. An ultra-sparse code underlies the generation of neural sequences in a songbird. *Nature* **419**, 65–70 (2002).
29. Margrie, T. W., Brecht, M. & Sakmann, B. *In vivo*, low-resistance, whole-cell recordings from neurons in the anaesthetized and awake mammalian brain. *Pflügers Arch.* **444**, 491–498 (2002).
30. Llinás, R. in *The Cerebellum: New Vistas* (eds Palay, S. L. & Chan-Palay, V.) 189–194 (Springer, New York, 1982).

Supplementary Information accompanies the paper on [www.nature.com/nature](http://www.nature.com/nature).

**Acknowledgements** We thank B. Clark, J. Davie, M. Farrant and A. Roth for comments. This work was supported by grants from the European Union (M.H.), Wellcome Trust (M.H. and T.W.M.), Gatsby Foundation (M.H.), NHMRC (T.W.M.) and by a UCL Graduate School Research Scholarship (P.C.). T.W.M. acknowledges the MPI für medizinische Forschung, Heidelberg, for support.

**Competing interests statement** The authors declare that they have no competing financial interests.

**Correspondence** and requests for materials should be addressed to M.H. ([m.hausser@ucl.ac.uk](mailto:m.hausser@ucl.ac.uk)).

## Birth of parthenogenetic mice that can develop to adulthood

Tomohiro Kono<sup>1,3</sup>, Yayoi Obata<sup>1,3</sup>, Quiong Wu<sup>1,3</sup>, Katsutoshi Niwa<sup>1,3</sup>, Yukiko Ono<sup>1</sup>, Yuji Yamamoto<sup>2,3</sup>, Eun Sung Park<sup>4</sup>, Jeong-Sun Seo<sup>4,5</sup> & Hidehiko Ogawa<sup>1,3</sup>

<sup>1</sup>Department of BioScience, and <sup>2</sup>Department of Applied Science, Tokyo University of Agriculture, Setagaya-ku, Tokyo 156-8502, Japan

<sup>3</sup>Bio-oriented Technology Research Advancement Institution (BRAIN), Minato-ku, Tokyo 105-0001, Japan

<sup>4</sup>MacroGen Inc, Chongno-Ku, Seoul 110-061, Korea

<sup>5</sup>Department of Biochemistry, Seoul National University College of Medicine, Chongno-Ku, Seoul 110-799, Korea

Only mammals have relinquished parthenogenesis, a means of producing descendants solely from maternal germ cells. Mouse parthenogenetic embryos die by day 10 of gestation<sup>1–4</sup>. Biparental reproduction is necessary because of parent-specific epigenetic modification of the genome during gametogenesis<sup>5–8</sup>. This leads to unequal expression of imprinted genes from the maternal and paternal alleles<sup>9</sup>. However, there is no direct evidence that genomic imprinting is the only barrier to parthenogenetic development. Here we show the development of a viable parthenogenetic mouse individual from a reconstructed oocyte containing two haploid sets of maternal genome, derived from non-growing and fully grown oocytes. This development was made possible by the appropriate expression of the *Igf2* and *H19* genes with other imprinted genes, using mutant mice with a 13-kilobase deletion in the *H19* gene<sup>10</sup> as non-growing oocytes donors. This full-term development is associated with a marked reduction in aberrantly expressed genes. The parthenote developed to adulthood with the ability to reproduce offspring. These results suggest that paternal imprinting prevents parthenogenesis, ensuring that the paternal contribution is obligatory for the descendant.

Maternal-specific *de novo* methylation of imprinted loci occurs during oocyte growth<sup>7,8,11,12</sup>; such non-growing oocytes from newborn mice are considered to be naive with respect to most of the maternal imprinting process. Parthenogenetic mouse embryos (ng<sup>wt</sup>/fg<sup>wt</sup>) that contain genomes from non-growing (ng<sup>wt</sup>) and fully grown (fg<sup>wt</sup>) oocytes can develop into 13.5-day-old fetuses<sup>12</sup>, by the appropriate expression of many imprinted genes<sup>13</sup>. However, the imprinted expression of the *H19* and *Igf2* genes has not been altered in the ng allele. The expression of the *Igf2* and *H19* genes are coordinately regulated by *cis*-acting elements, depending on the methylation status of the differentially methylated region (DMR) of the *H19* gene<sup>14–16</sup> and on endoderm-specific enhancers<sup>17</sup> (Fig. 1i). To block *H19* gene expression from ng oocyte alleles, mutant mice harbouring a 3-kilobase (kb) deletion in the *H19* transcription unit<sup>18</sup> were used to construct parthenogenetic embryos. The ng<sup>H19Δ3</sup>/fg<sup>wt</sup> parthenotes developed as live fetuses for 17.5 days of gestation, but showed no sign of further development<sup>19</sup>. The *Igf2*

Table 1 Development of reconstructed parthenogenetic embryos

Developmental progress	Number
Number of reconstructed eggs	457
Number of embryos developed to blastocysts	417 (91.2% of reconstructed eggs)
Number of embryos transferred	371 (89.0% of blastocysts)
Number pregnant/recipients	24/26
Number of implantation to recipients	246 (71.7% of embryos transferred to pregnant)
Number of pups	28 (8.2% of embryos transferred to pregnant)
Dead	18 (5.2% of embryos transferred to pregnant)
Live	8 (2.3% of embryos transferred to pregnant)
Survived	2 (0.6% of embryos transferred to pregnant)

gene, which encodes a growth-promoting factor (IGF-II), is well known as a major regulator of fetal growth<sup>10,18,20</sup>. These experiments suggest that the expression of *Igf2* along with monoallelic expression of the *H19* gene leads to further development of parthenotes.

First we investigated the development of the  $ng^{H19\Delta13}/fg^{wt}$  parthenogenetic embryos, which were expressing the *Igf2* gene from the *ng* allele. A total of 598  $ng^{H19\Delta13}/fg^{wt}$  oocytes were constructed by serial nuclear transfer<sup>12</sup> using *ng* oocytes from the *H19* <sup>$\Delta$ 13</sup> newborn mice<sup>10</sup>. After *in vitro* maturation and artificial activation, 78% of the oocytes resulted in diploid one-cell parthenogenetic embryos that formed two second polar bodies and pronuclei. Of the 457 eggs cultured *in vitro*, 91.2% developed to the morula/blastocyst stage (Table 1). In all, 371 morula/blastocysts derived from  $ng^{H19\Delta13}/fg^{wt}$  oocytes were transferred to 26 recipient females, and of these 24 became pregnant. Beyond our expectations, a total of 10 live and 18 dead pups were recovered by autopsy at 19.5 days of gestation (Fig. 1a–d). Of these, two individual pups were successfully restored, showing the apparently normal neonate morphology (Fig. 1a, b). To confirm that this unique phenomenon is seen only in  $ng^{H19\Delta13}/fg^{wt}$  parthenotes, we reassessed the development of  $ng^{H19\Delta3}/fg^{wt}$  parthenotes<sup>19</sup>. The data confirmed our previous results that  $ng^{H19\Delta3}/fg^{wt}$  parthenotes do not develop beyond day 17.5 of gestation (data not shown).

The body weights of the two surviving parthenogenetic pups were 1,372 and 1,310 mg (Fig. 1a, b), similar to those of the control

B6D2F1  $\times$  B6<sup>H19 $\Delta$ 13</sup> pups (mean  $\pm$  s.e.m,  $1,326 \pm 30$  mg,  $n = 12$ ). Polymerase chain reaction (PCR) analysis using specific primers for the *H19* gene and the *neo* cassette sequence revealed that they originated from  $ng^{H19\Delta13}/fg^{wt}$  embryos (Fig. 1h). One of the two survivors was nursed by a foster mother, and grew to adulthood. She was named ‘Kaguya’ (Fig. 1a, e) and showed normal reproductive performance: after mating she conceived and delivered normal pups (Fig. 1e). The other survivor was used for gene expression analysis on the day of recovery. The remaining live (Fig. 1c) and dead (Fig. 1d) pups at recovery showed developmental retardation, the live pups dying within 15 min. The mean body weight (Fig. 1f) was  $744 \pm 25$  mg ( $n = 8$ ) in live pups and  $786 \pm 20$  mg ( $n = 14$ ) in dead pups, and the developmental stage was estimated to be stage 26, as represented by day 18 fetuses<sup>21</sup>.

Histological analysis showed immaturity of the liver in the growth-retarded  $ng^{H19\Delta13}/fg^{wt}$  parthenotes. The sinusoids were packed with blood precursors, such as megakaryocytes, and erythroid and myeloid precursors, but the hepatic vein was not well differentiated (data not shown). The placenta was afflicted with atrophy (Fig. 1g) and the placental weights were 77 and 103 mg for the two survivors. However, gross abnormal formations of the spongiotrophoblast and labyrinth layer<sup>19</sup> were not observed, suggesting that the placenta was functionally capable of supporting embryo development.

To explore and compare features of the parthenotes, we carried out global gene expression analysis by oligonucleotide mouse 11K

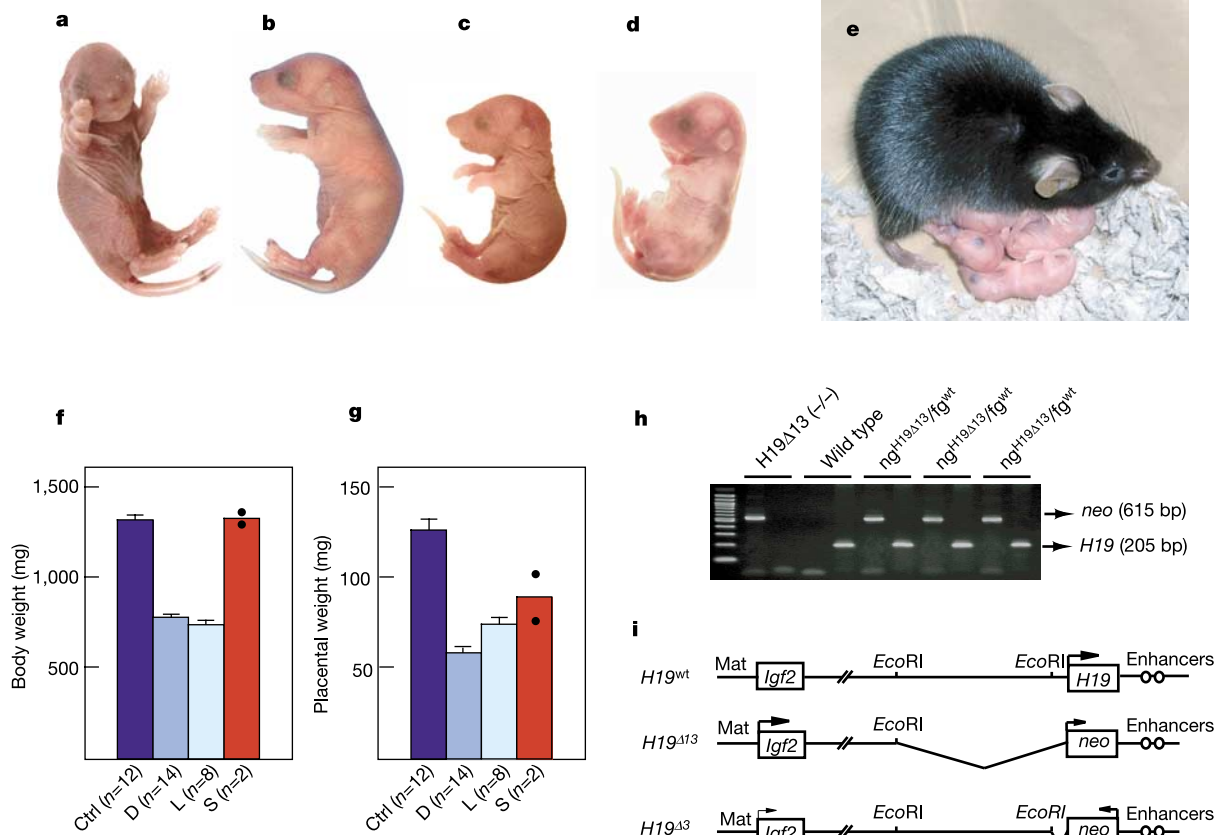


**Figure 1** Parthenogenetic mice derived from  $ng^{H19\Delta13}/fg^{wt}$  embryos. **a, b**, Parthenogenetic pups at birth with normal phenotypes. Of these the pup shown in **a** grew up a normal adult with reproductive competence (see **e**), and that in **b** was used for gene expression analysis. **c, d**, Growth-retarded parthenotes at day 19.5 of gestation, which died soon after the pup shown in **c** and just before that in **d**. **f, g**, Body (**f**) and placental (**g**) weights of the parthenotes at birth (Ctrl, controls  $n = 12$ ; D, dead at birth  $n = 14$ ; L, alive at birth  $n = 8$ ; S, survived  $n = 2$ ). Values are means  $\pm$  s.e.m. Dots on

column S represent the individual weights of the survivors. **h**, Genotype analysis by PCR showing the parthenotes containing an *ng* allele in which the *H19* gene was deleted with the *neo* cassette and an *fg* allele of the wild type. **i**, Schematic representation of the *H19*–*Igf2* locus in *H19*<sup>wt</sup>, *H19* <sup>$\Delta$ 13</sup> (ref. 10) and *H19* <sup>$\Delta$ 3</sup> (ref. 18) mutants. Only maternal alleles of each mutant are shown. The *H19* <sup>$\Delta$ 13</sup> mutant mice were used in the present study and the *H19* <sup>$\Delta$ 3</sup> mutants were used in our previous manuscript. The *EcoRI* fragment (–10 kb to –50 base pairs) contains the differentially methylated region.

microarray at day 12.5 of gestation. The phenotypes were similar to those of the control fetuses (Fig. 2a–c), although the fetal and placental weights of parthenotes were significantly lower than those of the controls (Fig. 2g, h). Interestingly, the umbilical cord was of normal thickness in the  $ng^{H19\Delta13}/fg^{wt}$  parthenotes, but was very poor in the  $ng^{wt}/fg^{wt}$  parthenotes (Fig. 2d–f). The proportion of embryos developing to day 12.5 of gestation was not significantly different between  $ng^{H19\Delta13}/fg^{wt}$  (35%, 16/46) and  $ng^{wt}/fg^{wt}$  (25%, 14/56) embryos. Clustering of the expression data and imaging were done using the Cluster and TreeView programs<sup>22</sup>, respectively. The gene expression profiles of the  $ng^{H19\Delta13}/fg^{wt}$  parthenotes differed from that of the  $ng^{wt}/fg^{wt}$  parthenotes, over a wide range of genes (Supplementary Fig. S1). For 1,038 genes, statistical significance was shown at the nominal significance level ( $P < 0.001$ ) of each univariate test. By ontology comparison, these genes can be classified into three categories: cell communication (15.1%), cell growth/maintenance (19.1%) and metabolism (21.9%) (Supplementary Fig. S2). These results suggest that the extended development in

the  $ng^{H19\Delta13}/fg^{wt}$  parthenotes is the product of a wide-ranging alteration of gene expression.

The oligonucleotide microarray analysis also showed that in the  $ng^{H19\Delta13}/fg^{wt}$  parthenotes, normalization occurred in all of the imprinted genes analysed (Supplementary Fig. S3). Out of 34 imprinted genes, only two genes, *Grb10* and *Nnat*, were respectively up- and downregulated at more than double and less than half the level in controls. However, 11 of the genes were downregulated and one gene, *Grb10*, was upregulated in the  $ng^{wt}/fg^{wt}$  parthenotes. Furthermore, the number of genes that were expressed differentially at a level greater than twofold ( $\log_2$  (Cy5/Cy3) ratio  $> +1$  and  $< -1$ ) compared with controls for each fetus, ranged from only 11 to 42 (average 30) in the  $ng^{H19\Delta13}/fg^{wt}$  parthenotes (Supplementary Fig. S4). In contrast, in the  $ng^{wt}/fg^{wt}$  parthenotes, a remarkably large number of genes, ranging from 431 to 1,324 (average 842), showed differential expression. Of these, *Dlk1* is the only gene that displayed changes in expression in all four  $ng^{H19\Delta13}/fg^{wt}$  parthenotes, whereas a common set of 329 genes with varied expression was found in the  $ng^{wt}/fg^{wt}$  parthenotes. When  $ng^{H19\Delta13}/fg^{wt}$  and  $ng^{wt}/fg^{wt}$  parthenotes were compared with each other, from 131 to 295 (average 208) genes displayed greater than twofold changes. Thus, the data clearly show that a marked normalization of expression of a wide-range of genes occurred in the  $ng^{H19\Delta13}/fg^{wt}$  parthenotes, and the more physiological pattern of gene expression provided sufficient developmental competence for these parthenotes.

To address the question of which genes have a key role in the survival of the reconstructed parthenotes, we focused on two pairs of interrelated genes: *Igf2* and *H19* (refs 10, 14–18), and *Dlk1* and *Gtl2* (refs 23–27) (Fig. 3), which are imprinted during spermatogenesis. Quantitative gene expression analysis by real-time RT–PCR (PCR with reverse transcription) showed that both *Igf2* and *H19*

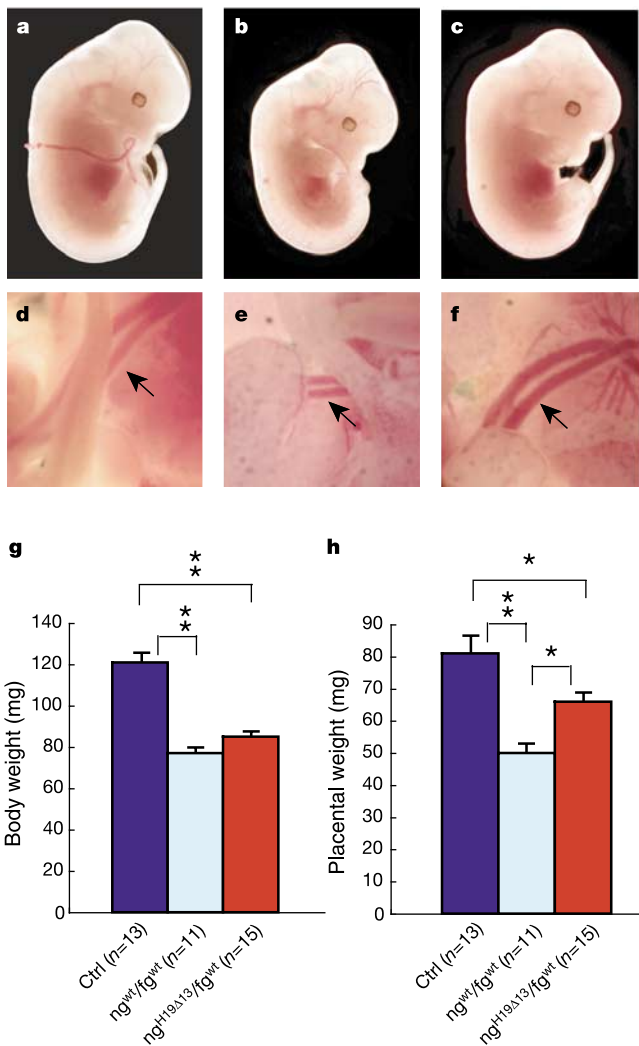


**Figure 2** Parthenogenetic fetuses at day 12.5 of gestation. **a, d**, Fetuses and the umbilical cords derived from control fertilized embryos; **b, e**,  $ng^{wt}/fg^{wt}$  parthenogenetic embryos; **c, f**,  $ng^{H19\Delta13}/fg^{wt}$  parthenogenetic embryos. Note that the umbilical cord (indicated by arrows) was well developed in the  $ng^{H19\Delta13}/fg^{wt}$  fetus (**f**) but was very poor in the  $ng^{wt}/fg^{wt}$  parthenote. **g, h**, Graphical representations of body (**g**) and placental (**h**) weights. Values are means  $\pm$  s.e.m. Significant differences at \*  $P < 0.05$  and \*\*  $P < 0.01$ .

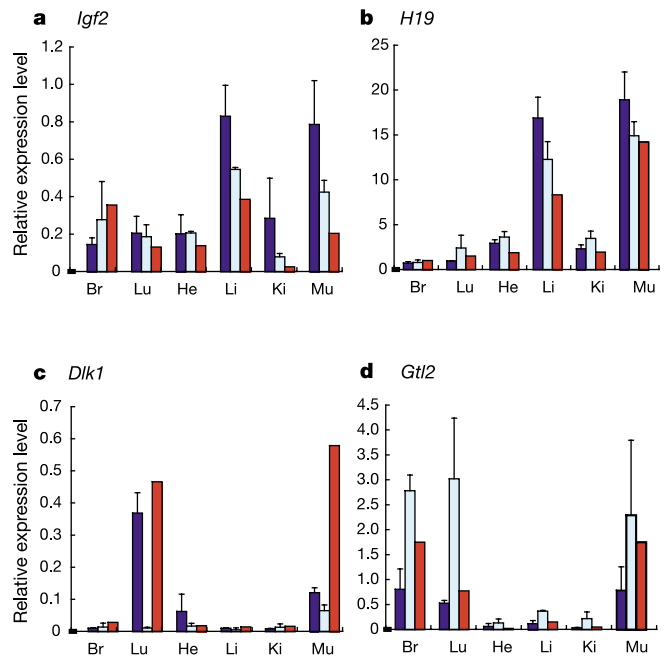


**Figure 3** Graphical representations of the expression of the two sets of coordinate imprinted genes in parthenogenetic fetuses. The expressions of four imprinted genes, **a**, *Igf2*; **b**, *H19*; **c**, *Dlk1*; and **d**, *Gtl2* in six different tissues of 19.5-day  $ng^{H19\Delta13}/fg^{wt}$  fetuses were analysed by quantitative real-time PCR. Br, brain; Lu, lung; He, heart; Li, liver; Ki, kidney; Mu, muscle. The values represent the levels of expression relative to that of the internal control gene (*Gapdh*). Control ( $n = 3$ ; dark blue); growth-retarded  $ng^{H19\Delta13}/fg^{wt}$  parthenogenetic pups ( $n = 3$ ; light blue); and survived  $ng^{H19\Delta13}/fg^{wt}$  parthenogenetic pup ( $n = 1$ ; red). Values are means  $\pm$  s.e.m.

genes were expressed at similar levels in the major organs of the ng<sup>H19Δ13</sup>/fg<sup>wt</sup> parthenote, as expected, because the *H19* transcription unit and its DMR had been deleted in the ng allele<sup>10</sup>. Interestingly, the *Gtl2* gene in the growth-retarded parthenotes was expressed at a level two- to fourfold higher than in the controls in all tissues analysed. Analysis using a DNA polymorphism present in the alleles of JF1 (*Mus musculus molossinus*) mice revealed that the *Gtl2* gene was biallelically expressed (data not shown). The *Dlk1* gene, which was expressed mainly in the lung, heart and muscle in the controls, was expressed in the lung and muscle in the ng<sup>H19Δ13</sup>/fg<sup>wt</sup> parthenotes. However, in the growth-retarded parthenotes, the expression in the lung was repressed. These expression patterns were confirmed by *in situ* hybridization at day 12.5 of gestation (data not shown). The decrease in *Gtl2* gene expression and activation of the *Dlk1* gene may be one of the causes of normal development of the survivor parthenotes. These genes are known to cause fetal lethality in the mutants<sup>25</sup>. Moreover, the maternal disomy mice for distal chromosome 12, where *Dlk1* and *Gtl2* are located, die perinatally with growth retardation<sup>26,27</sup>. Therefore, appropriate expression of *Dlk1* and *Gtl2* genes<sup>23–25</sup> may lead to even greater improvements in the efficiency of parthenogenetic development in mice.

Our study shows that imprinting is a barrier to parthenogenetic development in mice. This is consistent with the ‘parental conflict hypothesis’ (ref. 28), which proposes opposite effects of the parental genomes, such as in growth regulation during development. By increasing the activity of the *Igf2* gene in parthenogenetic embryos together with monoallelic expression of the *H19* gene, we have shown for the first time that it is possible to obtain a viable adult mouse from two maternal genomes. The most fascinating riddle arising from these results is how appropriate expression of the *Igf2* and *H19* genes caused the modification of a wide range of genes and normal development in the ng<sup>H19Δ13</sup>/fg<sup>wt</sup> parthenotes. The better development might lead to altered signalling, which then affects the expression of many other genes; however, the underlying mechanism is still unclear. Nevertheless, this study emphasizes the fact that normal development in mice is subject to a rigorous ‘conflict’ and differences due to imprinting of maternal and paternal genomes<sup>29,30</sup>. □

## Methods

### Oocyte manipulations

Fully-grown germinal vesicle (GV) oocytes were collected from the ovarian follicles of B6D2F1 (C57BL/6J × DBA) females 44–48 h after an equine chorionic gonadotrophin (eCG) injection. Ovulated MII oocytes were also collected from superovulated B6D2F1 mice 16 h after human chorionic gonadotrophin (hCG) injection. Mice harbouring a deletion of the *H19* transcription unit with DMR<sup>10</sup> (total 13 kb), which were kindly donated by S. Tilghman, were used as ng-stage oocyte donors. The mutant mice were originally produced by injection of targeted CCE ES cells into C57BL/6J blastocysts, and the founder mutants were backcrossed with C57BL/6J females. Ng oocytes, which were at the diplotene stage of the first meiosis, were collected from the ovaries of 1-day-old newborn mice.

Nuclear transfer was carried out as outlined previously<sup>12,19</sup>. Oocytes containing a haploid set of genomes from *H19*<sup>Δ13</sup> null mutant females and another genome from ovulated MII oocytes of wild-type B6D2F1 mice were constructed by serial nuclear transfer. Fusion of the diplotene oocytes with enucleated GV oocytes was induced with an inactivated Sendai virus (HVJ, 2,700 haemagglutinating activity units per ml). After fusion, the reconstituted oocytes were cultured for 14 h in α-MEM medium (Gibco). The GV oocytes were manipulated in a medium containing 200 μM dbcAMP and 5% calf serum throughout the experiment and were released from this medium 1 h after fusion with a ng-stage oocyte. A set of MII chromosomes from the reconstituted oocytes was again transferred into an enucleated MII oocyte. Then the reconstructed oocytes were artificially activated with 10 mM SrCl<sub>2</sub> in Ca<sup>2+</sup>-free M16 medium for 2 h. These embryos were cultured in M16 medium for 3 days in an atmosphere of 5% CO<sub>2</sub>, 5% O<sub>2</sub> and 90% N<sub>2</sub> at 37 °C. Blastocysts obtained from the constructed oocytes were transferred into the uterine horns of CD-1 female mice at 2.5 days of pseudopregnancy. The postimplantation development was assessed by an autopsy performed at 19.5 days of gestation.

### Oligonucleotide microarray analysis

Briefly, RNA was prepared from whole embryos using the RNeasy Midi Kit according to the manufacturer’s instructions (Qiagen). First-strand complementary DNA synthesis from 5 μg total RNA was done at 42 °C for 1 h, followed by second-strand cDNA synthesis

at 16 °C for 2 h. RNase I digestion was followed by proteinase K treatment. The resulting double-stranded cDNA was purified using the RNeasy Mini Kit according to the manufacturer’s instructions (Qiagen). Fluorescence-labelled RNA was generated by carrying out an *in vitro* transcription reaction (40 mM Tris-HCl, pH 7.5, 7 mM MgCl<sub>2</sub>, 10 mM NaCl, 2 mM spermidine, 5 mM dithiothreitol, 7.5 mM each of ATP, CTP and GTP, 5 mM UTP, 20 units RNase inhibitor and 1,000 units T7 RNA polymerase) at 37 °C for 4 h. This reaction was done in the presence of fluorescence-labelled nucleotides (Amersham Pharmacia Biotech) to generate Cy3- or Cy5-labelled RNA. The labelled RNA was subsequently purified (Qiagen RNeasy Mini Kit) and chemically fragmented at 94 °C for 15 min in fragmentation buffer (20 mM Tris-acetate, pH 8.1, 50 mM potassium acetate, 15 mM magnesium acetate). The fragmented, Cy3- or Cy5-labelled complementary RNA (20 μg) was lyophilized, resolubilized in hybridization buffer (50% formamide, 50 mM sodium phosphate, pH 8.0, 6 × SSC, 5 × Denhardt’s Solution, 0.5% SDS), and hybridized to oligonucleotide mouse 11K microarrays (Macrogen) at 42 °C for 24 h. T7 RNA polymerase was purchased from Ambion; primers, RNase inhibitors and all other enzymes were purchased from Roche Molecular Biochemicals.

The Mouse 11K microarrays consist of 50-mer oligonucleotide probes that represent 11,376 mouse genes, including 8,996 known and 2,380 unknown genes (<http://www.macrogen.com/>). Arrays were washed in three consecutive steps with 2 × SSC/0.1% SDS, 1 × SSC and 0.5 × SSC and scanned. Scans were performed on a Generation III scanner (Amersham Pharmacia Biotech), and the expression value for each gene was calculated using Image 5.0 software (BioDiscovery Inc.). Minor differences in microarray intensities were normalized using the SMA R package (Statistics for Microarray Analysis <http://www.stat.berkeley.edu/users/terry/zarray/Software/smacode.html>) developed by S. Dudoit, Y. H. Yang, M. Callow and T. Speed. Analyses were performed using Cluster developed by M. Eisen<sup>27</sup> and BRB ArrayTools developed by R. Simon and A. Peng (<http://linus.nci.nih.gov/BRB-ArrayTools.html>).

### Quantitative gene expression analysis

Quantitative analysis of gene expression was performed by means of real-time PCR (LightCycler System, Roche Molecular Biochemicals) using a ready-to-use reaction mixture kit (LightCycler FirstStart DNA Master SYBR Green I, Roche Molecular Biochemicals). The primers used were as follows: *Igf2*, 5′-AGGGGAGCTTGTGACACG-3′ and 5′-GGGTATCTGGGGAAGTCGTC-3′; *H19*, 5′-CATGCTGGCCCTTTGAA-3′ and 5′-TTGGCTCCAGGATGATGT-3′; *Dlk1*, 5′-ACTTGGCTGGACCTGGAGAA-3′ and 5′-CTGTTGGTTCGGCTACGAT-3′; *Gtl2*, 5′-AAGCACCATGAGCCACTAGG-3′ and 5′-TTGCACATTTCCCTGTGGAC-3′; *Gapdh*, 5′-GTCTGGAGTCTACTGGTGC-3′ and 5′-GAGCCCTTCCACAATGCCAAA-3′.

Received 20 November 2003; accepted 10 February 2004; doi:10.1038/nature02402.

- Surani, M. A. H. & Barton, S. C. Development of gynogenetic eggs in the mouse: Implications for parthenogenetic embryos. *Science* **222**, 1034–1036 (1983).
- Surani, M. A. H., Barton, S. C. & Norris, M. L. Development of reconstituted mouse eggs suggests imprinting of the genome during gametogenesis. *Nature* **308**, 548–550 (1984).
- Surani, M. A. *et al.* Genome imprinting and development in the mouse. *Development (suppl.)*, 89–98 (1990).
- McGrath, J. & Solter, D. Completion of mouse embryogenesis requires both the maternal and paternal genomes. *Cell* **37**, 179–183 (1984).
- Brannan, C. I. & Bartolomei, M. S. Mechanisms of genomic imprinting. *Curr. Opin. Genet. Dev.* **9**, 164–170 (1999).
- Tilghman, S. M. The sins of the fathers and mothers: Genomic imprinting in mammalian development. *Cell* **96**, 185–193 (1999).
- Mann, J. R. Imprinting in the germ line. *Stem Cells* **19**, 287–294 (2001).
- Li, E. Chromatin modification and epigenetic reprogramming in mammalian development. *Nature* **3**, 662–673 (2002).
- Obata, Y. & Kono, T. Maternal primary imprinting is established at a specific time for each gene throughout oocyte growth. *J. Biol. Chem.* **277**, 5285–5289 (2002).
- Leighton, P. A., Ingram, R. S., Eggenschwiler, J., Efstratiadis, A. & Tilghman, S. M. Disruption of imprinting caused by deletion of the *H19* gene region in mice. *Nature* **375**, 34–39 (1995).
- Lucifero, D., Mertineit, C., Clarke, H. J., Bestor, T. H. & Trasler, J. M. Methylation dynamics of imprinted genes in mouse germ cells. *Genomics* **79**, 530–538 (2002).
- Kono, T., Obata, Y., Yoshimizu, T., Nakahara, T. & Carroll, J. Epigenetic modifications during oocyte growth correlates with extended parthenogenetic development in the mouse. *Nature Genet.* **13**, 91–94 (1996).
- Obata, Y. *et al.* Disruption of primary imprinting during oocyte growth leads to the modified expression of imprinted genes during embryogenesis. *Development* **125**, 1553–1560 (1998).
- Feil, R., Walter, J., Allen, N. D. & Reik, W. Developmental control of allelic methylation in the imprinted mouse *Igf2* and *H19* genes. *Development* **120**, 2933–2943 (1994).
- Thorvaldsen, J. L., Duran, K. L. & Bartolomei, M. S. Deletion of the *H19* differentially methylated domain results in loss of imprinted expression of *H19* and *Igf2*. *Genes Dev.* **12**, 3693–3702 (1998).
- Hark, A. T. *et al.* CTCF mediates methylation-sensitive enhancer-blocking activity at the *H19/Igf2* locus. *Nature* **405**, 486–489 (2000).
- Leighton, P. A., Saam, J. R., Ingram, R. S., Stewart, C. L. & Tilghman, S. M. An enhancer deletion affects both *H19* and *Igf2* expression. *Genes Dev.* **9**, 2079–2089 (1995).
- Ripoché, M. A., Kress, C., Poirier, F. & Dandolo, L. Deletion of the *H19* transcription unit reveals the existence of a putative imprinting control element. *Genes Dev.* **11**, 1596–1604 (1997).
- Kono, T., Sotomaru, Y., Katsuzawa, Y. & Dandolo, L. Mouse parthenogenetic embryos with monoallelic *H19* expression can develop to day 17.5 of gestation. *Dev. Biol.* **243**, 294–300 (2002).
- Wang, Z. Q., Fung, M. R., Barlow, D. P. & Wagner, E. F. Regulation of embryonic growth and lysosomal targeting by the imprinted *Igf2/Mpr* gene. *Nature* **372**, 464–467 (1994).
- Theiler, K. *The House Mouse: Atlas of Embryonic Development* 122–128 (Springer, Berlin, 1989).
- Eisen, M. B., Spellman, P. T., Brown, P. O. & Botstein, D. Cluster analysis and display of genome-wide expression patterns. *Proc. Natl Acad. Sci. USA* **95**, 14863–14868 (1998).

23. Schmidt, J. V., Matteson, P. G., Jones, B. K., Guan, X. J. & Tilghman, S. M. The Dlk1 and Gtl2 genes are linked and reciprocally imprinted. *Genes Dev.* **14**, 1997–2002 (2000).
24. Kobayashi, S. *et al.* Mouse Peg9/Dlk1 and human PEG9/DLK1 are paternally expressed imprinted genes closely located to the maternally expressed imprinted genes: mouse Meg3/Gtl2 and human MEG3. *Genes Cells* **5**, 1029–1037 (2000).
25. Lin, S. P. *et al.* Asymmetric regulation of imprinting on the maternal and paternal chromosomes at the Dlk1-Gtl2 imprinted cluster on mouse chromosome 12. *Nature Genet.* **35**, 97–102 (2003).
26. Georgiades, P., Watkins, M., Surani, M. A. & Ferguson-Smith, A. C. Parental origin-specific developmental defects in mice with uniparental disomy for chromosome 12. *Development* **127**, 4719–4728 (2000).
27. Georgiades, P., Watkins, M., Burton, G. J. & Ferguson-Smith, A. C. Roles for genomic imprinting and the zygotic genome in placental development. *Proc. Natl Acad. Sci. USA* **98**, 4522–4527 (2001).
28. Moore, T. & Haig, D. Genomic imprinting in mammalian development: a parental tug-of-war. *Trends Genet.* **7**, 45–49 (1991).
29. Reik, W. & Walter, J. Genomic imprinting: parental influence on the genome. *Nature Rev. Genet.* **2**, 21–32 (2001).
30. Murphy, S. K. & Jirtle, R. L. Imprinting evolution and the price of silence. *BioEssays* **25**, 577–588 (2003).

Supplementary Information accompanies the paper on [www.nature.com/nature](http://www.nature.com/nature).

**Acknowledgements** We thank A. Surani, Wellcome CRC Institute, J. Carroll, University College London and T. Moore, University College Cork, Ireland, for critical reading and discussions; O.-Y. Kwon, MacroGen, for microarray analysis; and T. Kumagai for technical assistance. This work was supported by grants from the Bio-oriented Technology Research Advancement Institution (BRAIN), Japan, and The Ministry of Education, Science, Culture and Sports of Japan.

**Competing interests statement** The authors declare that they have no competing financial interests.

**Correspondence** and requests for materials should be addressed to T.K. (tomohiro@nodai.ac.jp).

## Intracellular gate opening in Shaker K<sup>+</sup> channels defined by high-affinity metal bridges

Sarah M. Webster\*, Donato del Camino\*, John P. Dekker & Gary Yellen

Department of Neurobiology, Harvard Medical School, 220 Longwood Avenue, Boston, Massachusetts 02115, USA

\* These authors contributed equally to this work

Voltage-gated potassium channels such as Shaker help to control electrical signalling in neurons by regulating the passage of K<sup>+</sup> across cell membranes. Ion flow is controlled by a voltage-dependent gate at the intracellular side of the pore, formed by the crossing of four  $\alpha$ -helices—the inner-pore helices. The prevailing model of gating is based on a comparison of the crystal structures of two bacterial channels—KcsA in a closed state and MthK in an open state—and proposes a hinge motion at a conserved glycine that splays the inner-pore helices wide open<sup>1</sup>. We show here that two types of intersubunit metal bridge, involving cysteines placed near the bundle crossing, can occur simultaneously in the open state. These bridges provide constraints on the open Shaker channel structure, and on the degree of movement upon opening. We conclude that, unlike predictions from the structure of MthK, the inner-pore helices of Shaker probably maintain the KcsA-like bundle-crossing motif in the open state, with a bend in this region at the conserved proline motif (Pro-X-Pro) not found in the bacterial channels. A narrower opening of the bundle crossing in Shaker K<sup>+</sup> channels may help to explain why Shaker has an approximately tenfold lower conductance than its bacterial relatives.

The recent elucidation of four K<sup>+</sup> channel crystal structures has revealed the general architectural motifs in this large family of transmembrane proteins<sup>1–5</sup>. Each of the tetrameric structures has a

central pore formed by two transmembrane helices and a selectivity filter structure from each of the four subunits. The sequence homology in the family of K<sup>+</sup> channels is strongest in the region of the selectivity filter, a region that is crucial for allowing rapid and selective permeation of K<sup>+</sup> ions<sup>6</sup>. Structurally, the selectivity filter is nearly identical in the channels solved thus far. However, the structures reveal significant differences in the conformation of the inner-pore helices in the region of the intracellular gate.

On the basis of differences in inner-helix configuration between two types of bacterial K<sup>+</sup> channels, KcsA and MthK<sup>1,2,5</sup>, MacKinnon and colleagues proposed a general model of K<sup>+</sup> channel gating. In the apparently closed KcsA structure, the inner M2 helices are straight, and they cross in the lower part of the S6 to form an inverted teepee-like structure. Access from the intracellular surface to the pore is through a long, narrow, hydrophobic entrance. MthK, by contrast, was crystallized in conditions that favoured the open state of the channel. The inner helices are bent at Gly83, which splays them apart to form a wide inner pore, 12 Å across at its narrowest point. These two structures are proposed to represent the closed and open states. In the gating model, the inner helices would swing around the conserved glycine to move from the narrow, closed KcsA pore to the wide, open MthK pore. This structure-based gating model is appealing in its simplicity, but it does not fit with the details of functional experiments done on voltage-gated K<sup>+</sup> channels. Here we present a model of gating for a voltage-dependent K<sup>+</sup> channel based on constraints established by the state dependence of metal bridging at two engineered binding sites.

A cysteine replacement at Shaker V476 creates a high-affinity Cd<sup>2+</sup>-binding site that stabilizes an open state of the channel<sup>7</sup>. Cd<sup>2+</sup> binding prevents these channels from closing even at very negative voltages, apparently by forming a bridge between a cysteine in one subunit and a native histidine (H486) in a neighbouring subunit<sup>7</sup> (Fig. 1). Replacement of the native histidine with tyrosine, threonine or valine abolished this high-affinity Cd<sup>2+</sup> ‘lock-open effect’. Other ligand combinations (Cys–Cys, His–Cys, His–His)

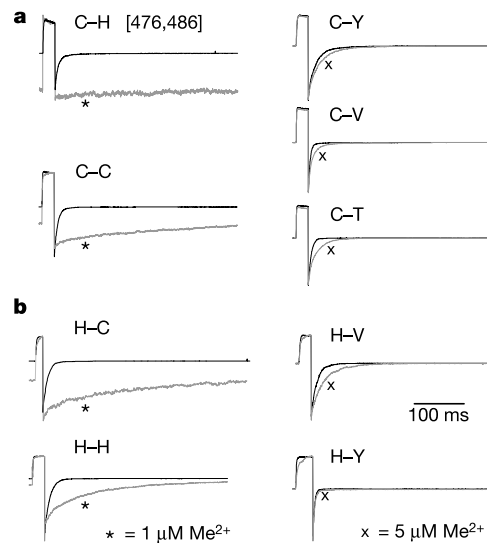


**Figure 1** The lock-open effect requires metal binding residues at positions 476 and 486. Channel currents measured in control solutions (black traces) or in the presence of **a**, Cd<sup>2+</sup> or **b**, Zn<sup>2+</sup> (grey traces). Lock-open (prevention or delay of closure) occurs only for channels with two metal-binding ligands (left column), whereas channels with only one metal-binding ligand (right column) show only a slight slowing of the tails. Activating steps to +60 mV were followed by closure at –110 mV (C–C, C–H, C–V and C–T), –140 mV (H–C, H–H, H–V and C–Y) or –180 mV (H–Y). Without metal, maximum outward currents ranged from 0.7 to 2.7 nA; with metal, outward currents (normalized in the figure) ranged from 15 to 37% of the control because of inactivation.